# SUPPORTING INFORMATION

## Understanding Yb$^{3+}$ sensitized photon avalanche in Pr$^{3+}$ co-doped nanocrystals: modelling and optimization

M.Dudek[1*], Z.Korczak[1], K.Prorok[1], O.Bezkrovnyi[1], L.Sun[3], M.Szalkowski[1,2*], A.Bednarkiewicz[1*]

1. Institute of Low Temperature and Structure Research, Polish Academy of Sciences, ul. Okólna 2, 50-422 Wroclaw, Poland
2. Nanophotonics Group, Institute of Physics, Faculty of Physics Astronomy and Informatics, Nicolaus Copernicus University in Toruń, ul. Grudziądzka 5, 87-100 Toruń, Poland
3. Department of Chemistry, College of Sciences, Shanghai University, Shanghai 200444, China

Corresponding author: m.dudek@intibs.pl, a.bednarkiewicz@intibs.pl;
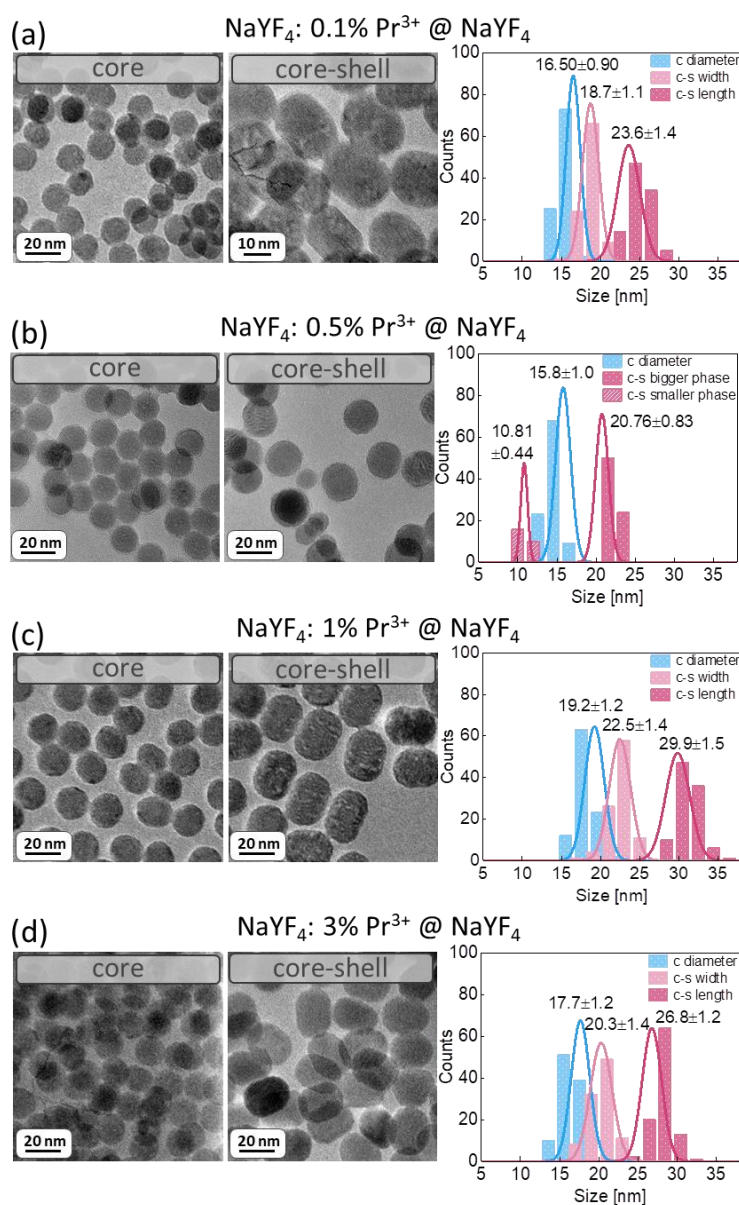


**Figure S1. Morphology characteristic of β-NaYF₄ nanocrystals:** TEM images and histograms with average sizes of core (c) and core-shell (c-s) nanocrystals singly doped with *(a)* 0.1%, *(b)* 0.5%, *(c)* 1% and *(d)* 3% of Pr$^{3+}$ ions.

**Table S1**. Average dimensions and shell thicknesses for samples presented in the **Figure S1**.

| Dopant: | Average core diameter [nm] | Average core-shell width [nm] | Average core-shell length [nm] | Average shell thickness in width [nm] | Average shell thickness in length [nm] |
|---|---|---|---|---|---|
| 0.1% $Pr^{3+}$ | 16.50±0.90 | 18.7±1.1 | 23.6±1.4 | 1.1±1.0 | 3.6±1.2 |
| 0.5% $Pr^{3+}$ | 15.8±1.0 | 20.76±0.83 | | 2.50±0.91 | |
| 1% $Pr^{3+}$ | 19.2±1.2 | 22.5±1.4 | 29.9±1.5 | 1.7±1.3 | 5.4±1.4 |
| 3% $Pr^{3+}$ | 17.7±1.2 | 20.3±1.4 | 26.8±1.2 | 1.3±1.3 | 4.6±1.2 |
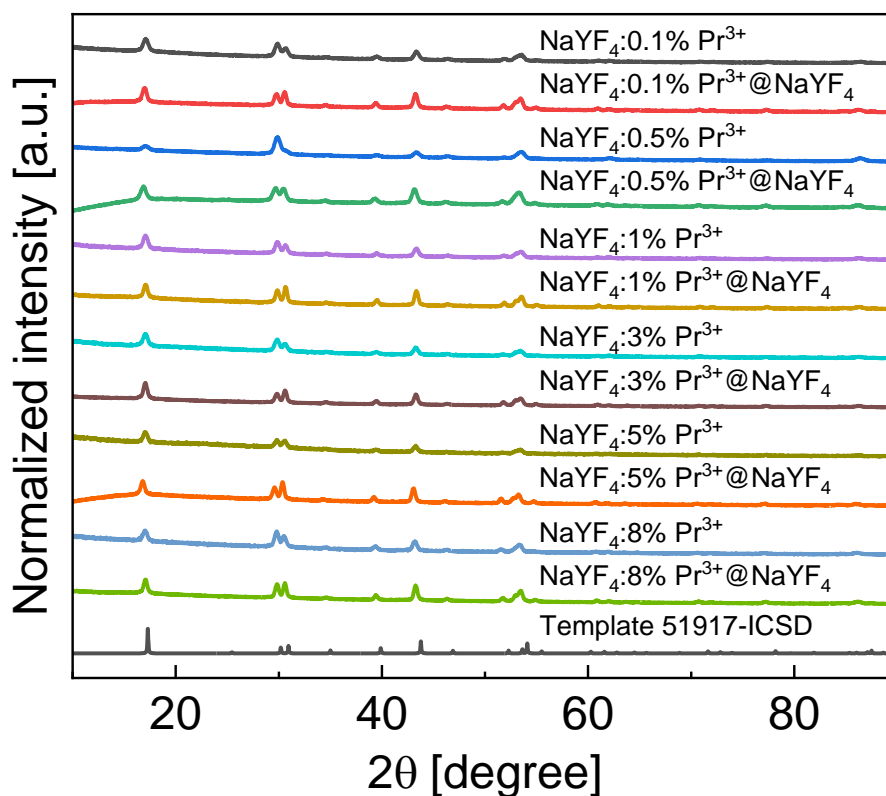


**Figure S2**. X-ray powder diffraction for core and core-shell $NaYF_4$ nanocrystals singly doped with 0.1%, 0.5%, 1%, 3%, 5% and 8% of $Pr^{3+}$ ions as well as the template of the β-$NaYF_4$.
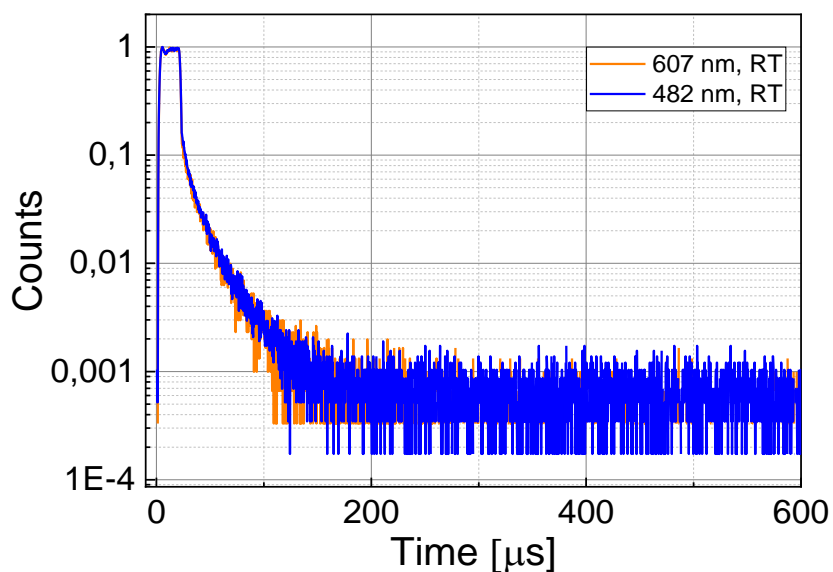
**Figure S3**. Conventional fluorescence lifetime curves for NaYF$_4$:0.5 % Pr$^{3+}$, 15% Yb$^{3+}$ @ NaYF$_4$ nanocrystals measured at 482 nm (blue curve) and 607 nm (orange curve) at room temperature. Excitation wavelength 444 nm.
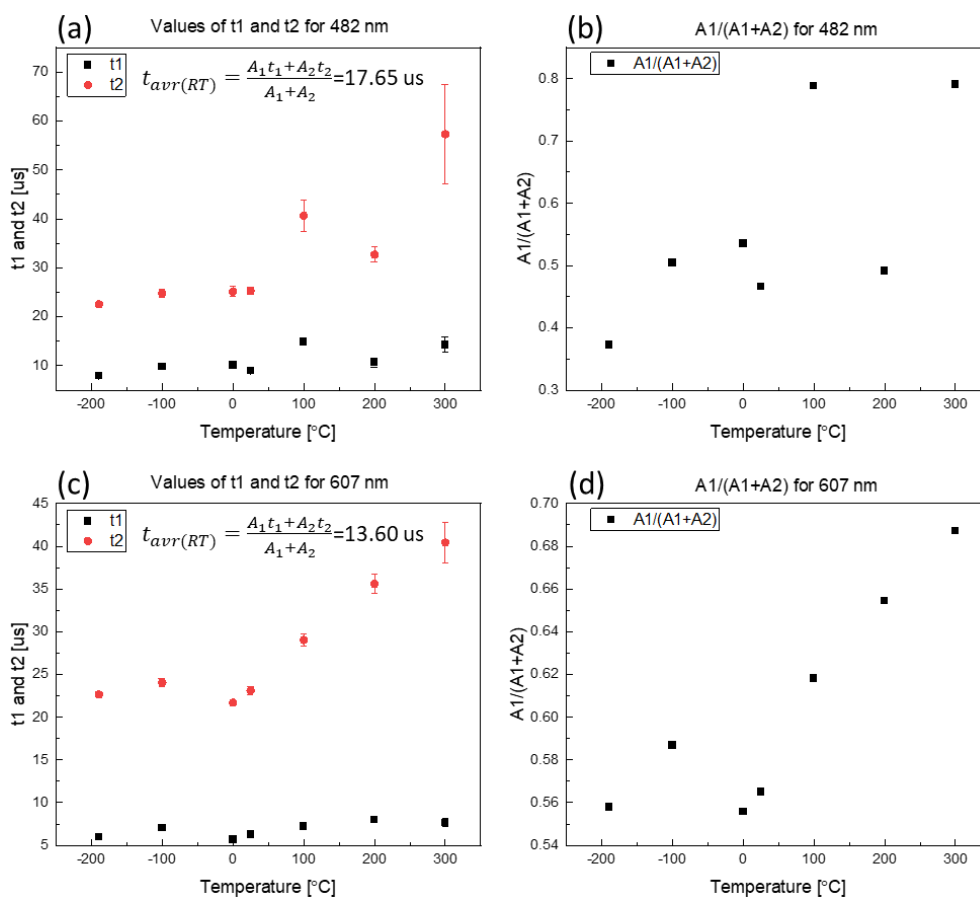


**Figure S4**. Parameters of short and long components of fluorescence lifetime decay curves for NaYF$_4$:0.5%Pr$^{3+}$,15%Yb$^{3+}$@NaYF$_4$ nanocrystals measured at wide range of temperatures at *(a-b)* 482 nm and *(c-d)* 607 nm.
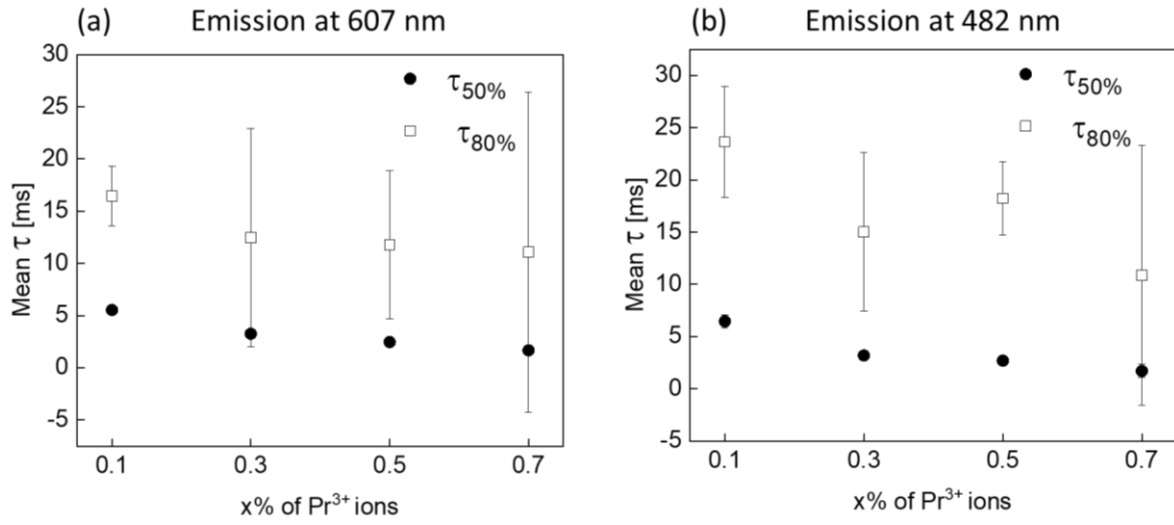
**Figure S5.** Average values of $\tau_{50\%}$ and $\tau_{80\%}$ for core-shell samples co-doped with 15%Yb$^{3+}$ and x% of Pr$^{3+}$ ions. Emission at *(a)* 607 nm and *(b)* 482 nm, respectively.

**Table S2.** Average maximum slopes and average thresholds values with standard deviations for samples co-doped with 15% Yb$^{3+}$ and 0.1%, 0.3%, 0.5% and 0.7% of Pr$^{3+}$ ions for emission at 482 and 607 nm.

| Emission at 482 nm | | |
|---|---|---|
| Sample | Average maximum S | Average $PA_{TH}$ [kW/cm$^2$] |
| NaYF$_4$:0.1%Pr | 5.09 ± 0.14 | 523 ± 23 |
| NaYF$_4$:0.3%Pr | 7.23 ± 0.21 | 591 ± 37 |
| NaYF$_4$:0.5%Pr | 7.97 ± 0.78 | 654 ± 218 |
| NaYF$_4$:0.7%Pr | 8.3 ± 1.1 | 817 ± 130 |
| NaYF$_4$:0.1%Pr@NaYF$_4$ | 6.59 ± 0.20 | 315 ± 64 |
| NaYF$_4$:0.3%Pr@NaYF$_4$ | 8.20 ± 0.40 | 284 ± 69 |
| NaYF$_4$:0.5%Pr@NaYF$_4$ | 9.02 ± 0.13 | 281.3 ± 2.9 |
| NaYF$_4$:0.7%Pr@NaYF$_4$ | 8.87 ± 0.54 | 650 ± 147 |
| Emission at 607 nm | | |
| Sample | Average maximum S | Average $PA_{TH}$ [kW/cm$^2$] |
| NaYF$_4$:0.1%Pr | 4.79 ± 0.15 | 493.4 ± 7.5 |
| NaYF$_4$:0.3%Pr | 6.87 ± 0.33 | 533 ± 75 |
| NaYF$_4$:0.5%Pr | 8.40 ± 0.47 | 579 ± 214 |
| NaYF$_4$:0.7%Pr | 8.39 ± 0.47 | 776 ± 183 |
| NaYF$_4$:0.1%Pr@NaYF$_4$ | 6.22 ± 0.37 | 335 ± 42 |
| NaYF$_4$:0.3%Pr@NaYF$_4$ | 8.06 ± 0.26 | 358 ± 185 |
| NaYF$_4$:0.5%Pr@NaYF$_4$ | 8.60 ± 0.14 | 285.6 ± 6.1 |
| NaYF$_4$:0.7%Pr@NaYF$_4$ | 8.56 ± 0.21 | 629 ± 123 |

## Differential rate equations and modelling

$$\frac{dN_1}{dt} = -F * \sigma_{GSA} * N(1) - w71 * N(7) * N(1) + w64 * N(6) * N(4) - WCR1 * N(1) * N(5) - WCR2 * N(1) * N(3) + \frac{b51 * N(5)}{\tau_5}$$
$$+ \frac{b41 * N(4)}{\tau_4} + \frac{b31 * N(3)}{\tau_3} + \frac{N(2)}{\tau_2} * NR2 * N(2) \qquad Eq.\,S1$$

$$\frac{dN_2}{dt} = 2 * WCR2 * N(1) * N(3) + \frac{b42 * N(4)}{\tau_4} + \frac{b32 * N(3)}{\tau_3} - \frac{N(2)}{\tau_2} + NR32 * N(3) - NR2 * N(2) \qquad Eq.\,S2$$

$$\frac{dN_3}{dt} = -WCR2 * N(1) * N(3) + \frac{b53 * N(5)}{\tau_5} + \frac{b43 * N(4)}{\tau_4} - \frac{N(3)}{\tau_3} - NR32 * N(3) + NR4 * N(4) \qquad Eq.\,S3$$

$$\frac{dN_4}{dt} = F * \sigma_{GSA} * N(1) - F * \sigma_{ESA} * N(4) + w71 * N(7) * N(1) - w64 * N(6) * N(4) + w65 * N(6) * N(5) - w74 * N(7) * N(4) + 2$$
$$* WCR1 * N(1) * N(5) - \frac{N(4)}{\tau_4} + \frac{b54 * N(5)}{\tau_5} + NR54 * N(5) - NR4 * N(4) \qquad Eq.\,S4$$

$$\frac{dN_5}{dt} = w74 * N(7) * N(4) - w65 * N(6) * N(5) - WCR1 * N(1) * N(7) - \frac{N(5)}{\tau_5} + F * \sigma_{ESA} * N(4) - NR5 * N(5) \qquad Eq.\,S5$$

$$\frac{dN_6}{dt} = -F * \sigma_{Yb} * N(6) + \frac{N(7)}{\tau_{Yb}} + w71 * N(7) * N(1) - w64 * N(6) * N(4) - w65 * N(6) * N(5) + w74 * N(7) * N(4) \qquad Eq.\,S6$$

$$\frac{dN_7}{dt} = F * \sigma_{Yb} * N(6) - \frac{N(7)}{\tau_{Yb}} - w71 * N(7) * N(1) + w64 * N(6) * N(4) + w65 * N(6) * N(5) - w74 * N(7) * N(4) \qquad Eq.\,S7$$

Values of $N(x)$ correspond population of respective levels. F is a flux and was calculated as:

$$F = \frac{I_P}{E} = \frac{I_P * \lambda}{h * c} \qquad Eq.\,S8$$

where:

$I_P$ corresponds pump power density $\left[\frac{W}{cm^2}\right]$. $\lambda$ is an excitation wavelength (852 nm). Two remaining parameters, h and c, signify Plank constant $(6.626 \cdot 10^{-34}\, J \cdot s)$ and speed of light in vacuum $(299792458\, \frac{m}{s})$, respectively.

**Table S3.** Parameters adopted to solve the DRE with description, value and unit.

| Parameter | Description | Basic value | Unit | Reference or justification |
|---|---|---|---|---|
| $\tau_2{}^*$ | Lifetime of level $^3H_5$ in $Pr^{3+}$ ions | $125.6 \cdot 10^{-3}$ | s | [1] |
| $\tau_3{}^*$ | Lifetime of level $^3H_6$ in $Pr^{3+}$ ions | $52.4 \cdot 10^{-3}$ | s | [1] |
| $\tau_4$ | Lifetime of level $^1G_4$ in $Pr^{3+}$ ions | $128 \cdot 10^{-6}$ | s | [2] |
| $\tau_5$ | Lifetime of level $^3P_0$ in $Pr^{3+}$ ions | $30 \cdot 10^{-6}$ | s | [3] |
| $\tau_{Yb}$ | Lifetime of $^2F_{5/2}$ of $Yb^{3+}$ ions | $7.5 \cdot 10^{-4}$ | s | [4] |
| $NR_{54}{}^*$ | Rate of nonradiative transition $^3P_0 \rightarrow {}^1G_4$ in $Pr^{3+}$ | $3.84 \cdot 10^{-8}$ | $\frac{1}{s}$ | [5] |
| $NR_{43}{}^*$ | Rate of nonradiative transition $^1G_4 \rightarrow {}^3H_6$ in $Pr^{3+}$ | $1.15$ | $\frac{1}{s}$ | [5] |
| $NR_{32}{}^*$ | Rate of nonradiative transition $^3H_6 \rightarrow {}^3H_5$ in $Pr^{3+}$ | $89132.2$ | $\frac{1}{s}$ | [5] |

| | | | | |
|---|---|---|---|---|
| NR$_{21}$ | Rate of nonradiative transition $^3H_5 \rightarrow ^3H_4$ in Pr$^{3+}$ | 130321.7 | $\frac{1}{s}$ | 5 |
| W$_{71}$ | Rate of ET [Yb$^{3+}$:$^2F_{5/2}$, Pr$^{3+}$: $^3H_4$]$\rightarrow$[Yb$^{3+}$:$^2F_{7/2}$, Pr$^{3+}$: $^1G_4$] | 1.2·10$^{-16}$ | $\frac{cm^3}{s}$ | 6 |
| W$_{74}$ | Rate of ETU [Yb$^{3+}$:$^2F_{5/2}$, Pr$^{3+}$: $^1G_4$]$\rightarrow$[Yb$^{3+}$:$^2F_{7/2}$, Pr$^{3+}$: $^3P_1$] | 1.2·10$^{-16}$ | $\frac{cm^3}{s}$ | w74=w71 |
| W$_{64}$ | Rate of ET [Yb$^{3+}$:$^2F_{7/2}$, Pr$^{3+}$: $^1G_4$]$\rightarrow$[Yb$^{3+}$:$^2F_{5/2}$, Pr$^{3+}$: $^3H_4$] | 4·10$^{-18}$ | $\frac{cm^3}{s}$ | w64=w71/30 |
| W$_{65}$ | Rate of ETU [Yb$^{3+}$:$^2F_{7/2}$, Pr$^{3+}$: $^3P_1$]$\rightarrow$[Yb$^{3+}$:$^2F_{5/2}$, Pr$^{3+}$: $^1G_4$] | 1.6·10$^{-16}$ | $\frac{cm^3}{s}$ | 4 |
| W$_{CR1}$* | Rate of [$^3P_1$,$^3H_4$]$\rightarrow$[$^1G_4$, $^1G_4$] CR process in Pr$^{3+}$ | 1.1·10$^{-18}$ | $\frac{cm^3}{s}$ | 4 |
| W$_{CR2}$* | Rate of [$^3H_6$,$^3H_4$]$\rightarrow$[$^3H_5$, $^3H_5$] CR process in Pr$^{3+}$ | 1.1·10$^{-18}$ | $\frac{cm^3}{s}$ | WCR2=WCR1 |
| σ$_{ESA}$ | Absorption cross section of Pr$^{3+}$ ions from excited state | 0.7·10$^{-20}$ | $cm^2$ | 6 |
| σ$_{GSA}$* | Absorption cross section of Pr$^{3+}$ ions from ground state | 8·10$^{-27}$ | $cm^2$ | 4 |
| σ$_{Yb}$ | Absorption cross section of Yb$^{3+}$ ions | 8·10$^{-26}$ | $cm^2$ | 4 |
| b$_{51}$ | Branching ratio of emission from $^3P_0$ | 0.294 | - | Estimated from emission spectra |
| b$_{53}$ | Branching ratio of emission from $^3P_0$ | 0.686 | - | Estimated from emission spectra |
| b$_{54}$ | Branching ratio of emission from $^3P_0$ | 0.020 | - | Estimated from emission spectra |
| b$_{41}$ | Branching ratio of emission from $^1G_4$ | 0.061 | - | Estimated based on: 7 |
| b$_{42}$ | Branching ratio of emission from $^1G_4$ | 0.711 | - | Estimated based on: 7 |
| b$_{43}$ | Branching ratio of emission from $^1G_4$ | 0.228 | - | Estimated based on: 7 |
| b$_{31}$ | Branching ratio of emission from $^3H_6$ | 0.566 | - | 1 |
| b$_{32}$ | Branching ratio of emission from $^3H_6$ | 0.434 | - | 1 |

The rates of nonradiative transition were estimated on the basis of the chart of probabilities of nonradiative transitions of Ln$^{3+}$ ions in a tetragonal LiYF$_4$ laser crystal in a function of energy gap at T = 0 [5]. The probability of nonradiative transition from starting level, $J$, to the finished, $J'$, is described as $W_{JJ'}$. The data read from the chart were recalculated for room temperature according to the following equation appropriate for emission processes [8]:

$$W_{JJ'}(T) = W_{JJ'}(T = 0) \cdot (n + 1)^P \qquad Eq.S9$$

where

$$n = \left[exp\left(\frac{\hbar\omega}{k_B \cdot T}\right) - 1\right]^{-1} \qquad Eq.S10$$

$k_B$ is a Boltzman constant and equals 0.695 $cm^{-1} \cdot K^{-1}$. The $\hbar\omega$ corresponds the phonon energy in particular matrix (here $\hbar\omega = 350$ cm$^{-1}$), P indicates the number of phonons required for overcome appropriate energy gap ($\Delta E_{JJ'}$) :

$$P = \frac{\Delta E_{JJ'}}{\hbar\omega} \qquad\qquad Eq.\,S11$$

**Table S4.** Changes of values of DRE parameters used to check their influence of PA features. *Some parameters have been not influenced the PA.

| Parameter | Lower values | | Basic value | Higher values | | Unit |
|---|---|---|---|---|---|---|
| $\tau_2{}^*$ | No changes for values of the same order and an order of magnitude smaller | | $125.568\cdot10^{-3}$ | No changes for values of the same order and an order of magnitude bigger | | $s$ |
| $\tau_3{}^*$ | No changes for values of the same order, one and two orders of magnitude smaller | | $52.377\cdot10^{-3}$ | No changes for values of the same order, one and two orders of magnitude higher | | $s$ |
| $\tau_4$ | $70\cdot10^{-6}$ | $100\cdot10^{-6}$ | $128\cdot10^{-6}$ | $650\cdot10^{-6}$ | $3220\cdot10^{-6}$ | $s$ |
| $\tau_5$ | $1\cdot10^{-6}$ | $10\cdot10^{-6}$ | $30\cdot10^{-6}$ | $90\cdot10^{-6}$ | $120\cdot10^{-6}$ | $s$ |
| $\tau_{Yb}$ | $7.5\cdot10^{-5}$ | $3.5\cdot10^{-4}$ | $7.5\cdot10^{-4}$ | $9.5\cdot10^{-4}$ | $7.5\cdot10^{-3}$ | $s$ |
| $NR_{54}{}^*$ | No changes for values of the same order, one, two and three orders of magnitude smaller | | $3.84\cdot10^{-8}$ | No changes for values of the same order, one, two and three orders of magnitude bigger | | $\frac{1}{s}$ |
| $NR_{43}{}^*$ | No changes for values of the same order, one and two orders of magnitude smaller | | $1.15$ | No changes for values of the same order, one and two orders of magnitude higher. For values of four orders of magnitude bigger, changes were observed, however that big increase of NR43 make no sense. | | $\frac{1}{s}$ |
| $NR_{32}{}^*$ | Very minor change for smaller values. | | $89132.2$ | Lack of changes for bigger values. | | $\frac{1}{s}$ |
| $NR_{21}$ | $1303.217$ | $13032.17$ | $130321.7$ | Lack of changes for bigger values. | | $\frac{1}{s}$ |
| $W_{71}$ | $1.2\cdot10^{-17}$ | $0.2\cdot10^{-16}$ | $1.2\cdot10^{-16}$ | $2.3\cdot10^{-16}$ | $1.0\cdot10^{-15}$ | $\frac{cm^3}{s}$ |
| $W_{74}$ | $1.2\cdot10^{-17}$ | $0.2\cdot10^{-16}$ | $1.2\cdot10^{-16}$ | $2.3\cdot10^{-16}$ | $1.0\cdot10^{-15}$ | $\frac{cm^3}{s}$ |
| $W_{64}$ | $2\cdot10^{-19}$ | $1\cdot10^{-18}$ | $4\cdot10^{-18}$ | $8\cdot10^{-18}$ | $2\cdot10^{-17}$ | $\frac{cm^3}{s}$ |
| $W_{65}$ | $1.6\cdot10^{-17}$ | $0.5\cdot10^{-16}$ | $1.6\cdot10^{-16}$ | $5\cdot10^{-16}$ | $1.6\cdot10^{-15}$ | $\frac{cm^3}{s}$ |
| $W_{CR1}{}^*$ | No changes for values of the same order, one and two orders of magnitude smaller | | $1.1\cdot10^{-18}$ | No changes for values of the same order, one and two orders of magnitude higher | | $\frac{cm^3}{s}$ |
| $W_{CR2}{}^*$ | No changes for values of the same order, one and two orders of magnitude smaller | | $1.1\cdot10^{-18}$ | No changes for values of the same order, one and two orders of magnitude higher | | $\frac{cm^3}{s}$ |
| $\sigma_{ESA}$ | $0.2\cdot10^{-20}$ | $0.4\cdot10^{-20}$ | $0.7\cdot10^{-20}$ | $1.3\cdot10^{-20}$ | $2.5\cdot10^{-20}$ | $cm^2$ |

| | | | | | | |
|---|---|---|---|---|---|---|
| $\sigma_{GSA}$ * | No changes for values up to 3 orders of magnitude smaller | | $8 \cdot 10^{-27}$ | Very minor change for value two orders of magnitude higher. | | $cm^2$ |
| $\sigma_{Yb}$ | $8 \cdot 10^{-27}$ | $3 \cdot 10^{-26}$ | $8 \cdot 10^{-26}$ | $20 \cdot 10^{-26}$ | $30 \cdot 10^{-26}$ | $cm^2$ |
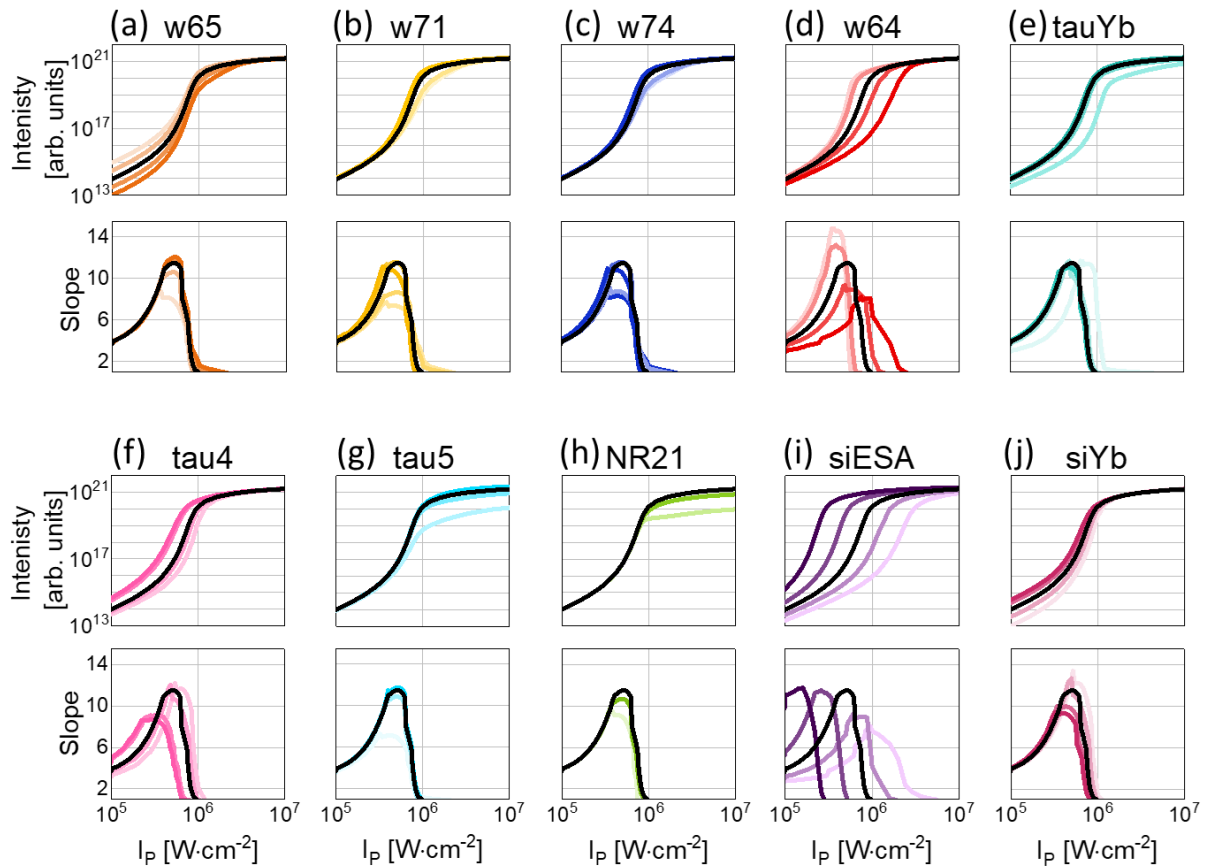


**Figure S6. Results from PA simulations for Pr³⁺, Yb³⁺ co-doped nanocrystals:** each panel contains two elements: simulated s-shaped dependences of luminescence intensity in a function of pump power density of the excitation laser and the corresponding slopes values of these s-shaped curves. The influence of changes of particular parameters, namely nonradiative transitions: *(a)* $w_{65}$, *(b)* $w_{71}$, *(c)* $w_{74}$, *(d)* $w_{64}$ *(h)* $NR_{21}$, radiative lifetimes: *(e)* $\tau_{Yb}$ *(f)* $\tau_4$, *(g)* $\tau_5$, and absorption cross sections: *(i)* $\sigma_{ESA}$, *(j)* $\sigma_{Yb}$ on PA futures are illustrated. Individual charts show, how the variation of these parameters affect the s-shape profiles and slope values. Saturated and desaturated colors correspond to increase or decrease of a given parameter value, respectively, as compared to pristine values (black).
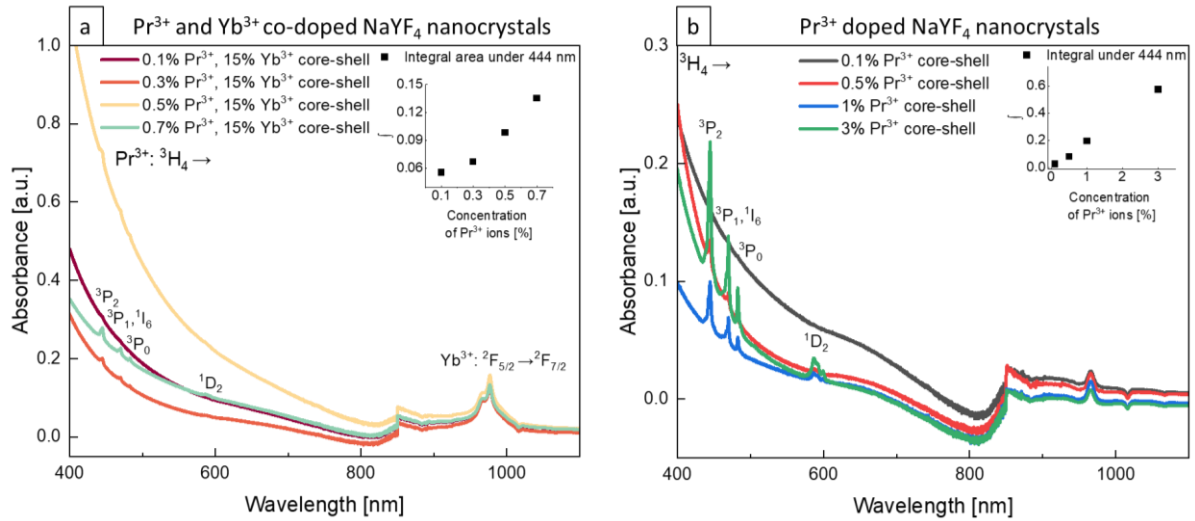
**Figure S7.** Absorption and scattering spectra of β-NaYF$_4$ nanocrystals: **(a)** co-doped with Pr$^{3+}$ and Yb$^{3+}$ **(b)** doped with Pr$^{3+}$ ions. Inserted charts in **(a)** and **(b)** present integral area under the peak at 444 nm.
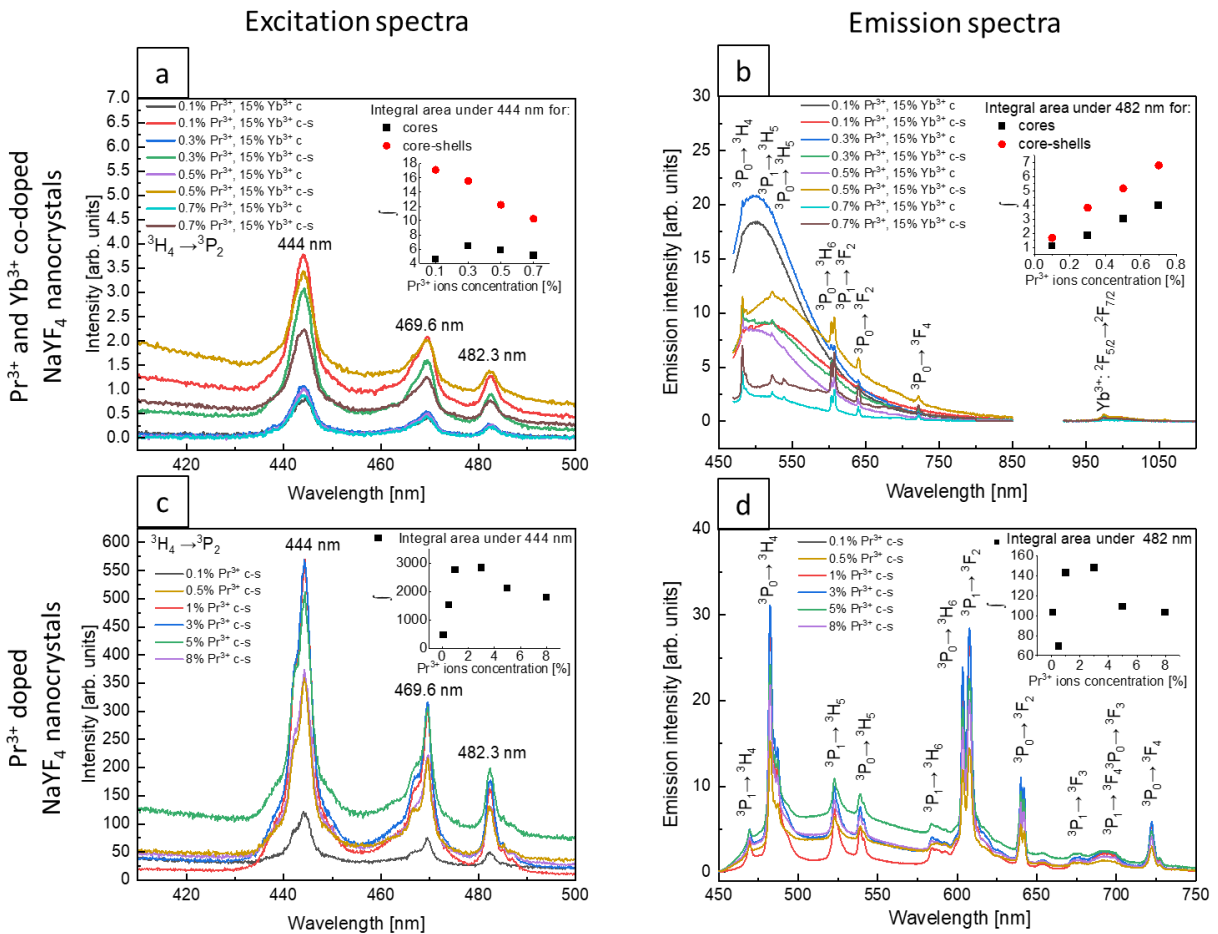


**Figure S8. Spectroscopic measurements for β-NaYF$_4$ nanocrystals**: excitation spectra for **(a)** cores and core-shells co-doped with Pr$^{3+}$ and Yb$^{3+}$ ions monitoring emission at 980 nm **(c)** core-shells doped with Pr$^{3+}$ ions monitoring emission at 607 nm; Emission spectra under excitation with 444 nm for **(b)** cores and core-shells co-doped with Pr$^{3+}$ and Yb$^{3+}$ ions **(d)** core-shells doped with Pr$^{3+}$ ions. Inserted plots: in excitation spectra show changes of the integral area under the peak at 444 nm with concentration of Pr$^{3+}$ ions for **(a)** core and core-shell samples co-doped with Pr$^{3+}$, Yb$^{3+}$ ions **(c)** core-shell singly Pr$^{3+}$ doped nanocrystals; in emission spectra show changes of the integral area under the peak at 482 nm with concentration of Pr$^{3+}$ ions for **(b)** core and core-shell samples co-doped with Pr$^{3+}$, Yb$^{3+}$ ions **(d)** core-shell singly Pr$^{3+}$ doped nanocrystals.

1      P. Babu and C. K. Jayasankar, *Physica B Condens Matter*, , DOI:10.1016/S0921-4526(01)00239-3.

2      B. E. Bowlby and B. Di Bartolo, *J Lumin*, 2002, **100**, 131–139.

3      P. Wu, B. Xiao, Q. Feng, X. Lin, W. Li, H. Xu and Z. Cai, *J Lumin*, 2021, **235**, 118028.

4      Y. Liang, Z. Zhu, S.  Qiao, S. Qiao, X. Guo, R. Pu, H. Tang, H. Liu, H. Dong, T. Peng, L.-D. Sun, J. Widengren and Q. Zhan, *Nature Nanotechnology 2022*, 2022, 1–7.

5      A. A. Kaminskii, *Crystlline Lasers: Physical Processes and Operating Schemes*, .

6      V. Lupei, *Spectrochim Acta A Mol Biomol Spectrosc*, 1998, **54**, 1615–1632.

7      Z. Wang, Z. Dai, S. Ji, S. Huang, B. Xiao, Z. He, H. Xu and Z. Cai, *J Lumin*, , DOI:10.1016/j.jlumin.2022.118870.

8      M. Szalkowski, M. Dudek, Z. Korczak, C. Lee, Ł. Marciniak, E. M. Chan, P. J. Schuck and A. Bednarkiewicz, *Optical Materials: X*, , DOI:10.1016/j.omx.2021.100102.